Generalized Abel transform for the analysis of fluid vibration in a tube

Minvydas Ragulskis
Kaunas University of Technology
Department of Mathematical Research in Systems
Studentu 50-222
Kaunas, Lithuania
E-mail: minvydas.ragulskis@ktu.lt

Arvydas Palevicius, MEMBER SPIE
Kaunas University of Technology
International Studies Center
Mickeviciaus 37
Kaunas, Lithuania

Liutauras Ragulskis
Vytautas Magnus University
Department of Informatics
Vileikos 8
Kaunas, Lithuania

Algimantas Bubulis
Kaunas University of Technology
Center of Mechatronics
Mickeviciaus 37
Kaunas, Lithuania

Abstract. Fluid vibrations in axisymmetric geometry according to the first harmonic in the circumferential direction are analyzed. This problem has a practical application in the analysis of transverse vibrations of fluid in an axisymmetric pipe. The numerical model is developed using finite-element techniques in axisymmetric geometry. Irrotational motions of ideal compressible fluid are analyzed. The finite-element model of the system is based on the approximation of nodal displacements via the shape functions. Thus the field of the amplitudes of the circumferential variation of the volumetric strain is calculated, exploiting conjugate approximation techniques. Obtained volumetric strains are used for the numerical construction of the interference pattern of the vibrating fluid. For this purpose the Abel transform, which is usually exploited in axisymmetric problems, is generalized for problems with circumferential variation of displacements. The obtained interference patterns are used in hybrid experimental–numerical procedures and help to interpret experimental results.
[DOI: 10.1117/1.2745820]

Subject terms: volumetric strain; time-average holography; vibration; Abel transform.

Paper 060548R received Jul. 11, 2006; revised manuscript received Nov. 3, 2006; accepted for publication Dec. 6, 2006; published online Jun. 5, 2007. This paper is a revision of a paper presented at the SPIE conference on Seventh International Conference on Vibration Measurements by Laser Techniques: Advances and Applications, Jun. 2006, Ancona, Italy. The paper presented there appears (unrefereed) in SPIE Proceedings Vol. 6345.

1 Introduction

In engineering, the integral Abel transform is often used in the analysis of spherically symmetric or axially symmetric objects. The Abel transform is used in different optical applications—from calculation of the radial mass distribution of galaxies[1] to sizing of microscopic droplets in emulsions.[2] The Abel transform plays a primary role in optical problems dealing with interpretation of fluid, gas, or even two-phase flow in circular transparent and semitransparent tubes.[3,4] Numerical techniques for interpretation of experimentally produced images involving Abel transforms are studied in Ref. 5. The term "generalized Abel integral transform" is used in Ref. 6, but there the authors consider the inverse Abel transform, and they apply spectral expansion using orthogonal functions and approximate numerical coefficients of the expansion.

The subject of our paper is the formation of optical fringes in a time-average hologram produced by vibrating fluid in axisymmetric tube. Thus the term "generalized Abel transform" is used here to highlight the fact that the analyzed axially symmetric medium is not constant in time. The Abel transform is generalized for measurement of dynamically varying processes. Such generalization is not trivial and requires appropriate modifications in the model of the optical system.

Development of hybrid numerical–experimental techniques is an important method of analysis used for interpretation and validation of experimental results,[7,8] especially when such experimental techniques as laser holography are applied for investigation of high-frequency vibrations of a fluid.[9,10] If the fluid dynamics is investigated in a tube, the problem becomes even more complicated, due to the complex geometry of the system. The Abel transform[11–13] must be exploited for the reconstruction of interference fringes, because the laser beam travels different distances through the fluid at different positions of the laser rays penetrating the surface of the tube. If the tube itself performs oscillations in the circumferential direction, the Abel transform must be generalized, and that is the main object of this paper.

Such problems of fluid dynamics in vibrating tubes are found in many engineering applications.[14–16] A typical example from biomedical applications is a problem when an ultrasonic probe is used to eliminate tissues, kidney stones, and clots of blood and their derivatives in arteries.[17] The energy of the ultrasonic probe is transferred in the form of high-frequency ultrasonic waves, which destroy certain tissues by local cavitation. Such ultrasonic devices can be exploited for destroying certain organic tissues for cancer therapy, clearing blocked blood vessels, etc.

Cavitation in a liquid, generated by an ultrasonic energy concentrator, produces microscopic steam bubbles. These bubbles expand and explode; the explosion destroys certain

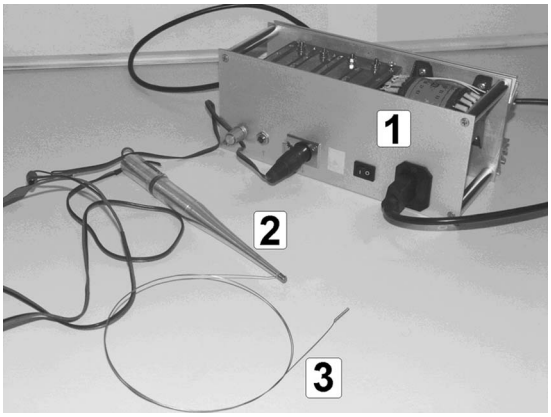

Fig. 1 The main parts of an ultrasonic probe: 1, generator; 2, ultrasonic wave concentrator; 3, working element (elastic steel wire waveguide).

tissues.[18] Usually longitudinal or tranverse waves are generated at the end of the ultrasonic probe. In order to expand the area of effective treatment, an elastic steel wire waveguide can be attached to the tip of the probe (Fig. 1). Ultrasonic vibrations are generated in the probe, and they are mechanically amplified by an exponential ultrasonic-wave concentrator and transferred to the elastic wire waveguide[19] (Fig. 2). Transverse standing waves in the waveguide produce cavitation at the antinodes of the wave when the wire is inserted into the fluid. Each antinode area around the waveguide can be used to destroy biological tissues. Unfortunately, the large gas–blood ratio that is generated in certain regimes of operation and caused by cavitation (Fig. 3) can impede the flow of oxygen-rich blood to vital organs and cause clots to form in blood vessels.[20]

The higher is the volumetric strain, the more effective is the treatment. But the volumetric strains must not exceed a certain critical value where the cavitation reaches a dangerous level. That critical value of volumetric strain can be calibrated and correlated with the number of interference fringes produced in a laser hologram of the fluid during laboratory experiments. Thus it is very important to perform accurate experimental investigations before such treatment can be used in real applications.

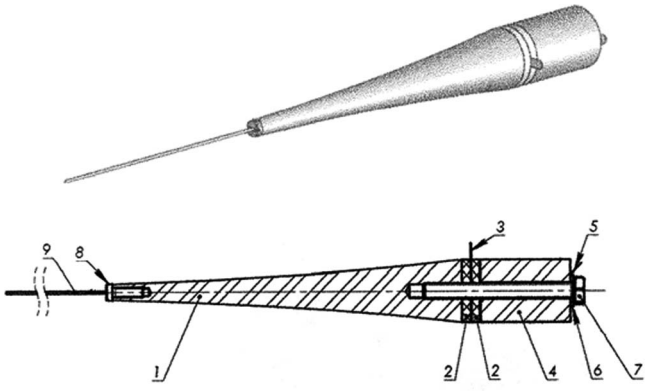

Fig. 2 Schematic diagram of the ultrasonic probe: 1, wave concentrator; 2, piezoelectric ceramics; 3, electrode; 4, ballast mass; 5, electrode; 6, disk washer; 7, bolt; 8, connector; 9, working element.

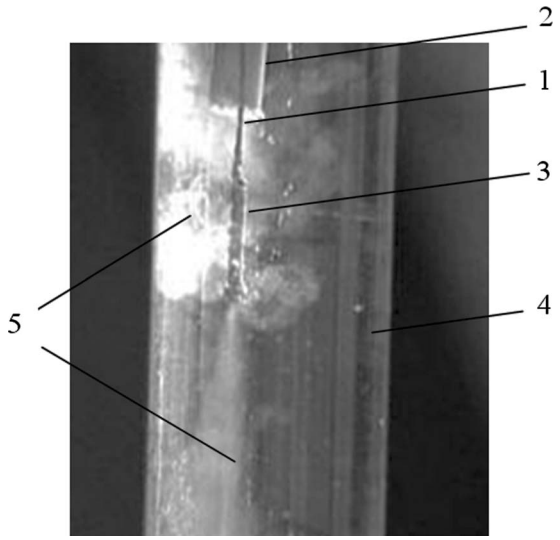

Fig. 3 Cavitation clouds in water generated by the ultrasonic probe: 1, waveguide; 2, flexible tubing; 3, catheter mounted on the end of the waveguide; 4, glass tube; 5, cavitation clouds.

The main goal of this paper is to show that interpretation of measurement results on vibrating fluid in axisymmetric geometry is neither trivial nor straightforward; misinterpretation of experimental data can lead to serious consequences in the context of the previously described ultrasonic probe treatment. The paper comprises several successive sections. First, a numerical model for an ideal compressible fluid without rotation is developed in axisymmetric geometry. Then the relationship between the intensity of a laser beam in the hologram plane and the volumetric strain in a vibrating fluid is developed. After that, the Abel transform is generalized in order to evaluate the effect of oscillating volumetric strain in axisymmetric geometry. Finally, results of numerical and experimental investigations are discussed, and conclusions are presented.

2 Model of the System

The numerical model of the fluid is developed on the basis of the finite-element model described in Refs. 21 and 22. First of all, the finite-element model for an ideal compressible fluid without rotation is developed in axisymmetric geometry for the motion according to the first harmonic in the circumferential direction. It is assumed that the angular frequency of excitation coincides with the eigenfrequency of the appropriate eigenmode, and thus the appropriate eigenproblem is analyzed. It is assumed that

$$u(x,y,\Theta) = \bar{u}(x,y)\cos\Theta,$$

$$v(x,y,\Theta) = \bar{v}(x,y)\cos\Theta,$$

$$w(x,y,\Theta) = \bar{w}(x,y)\sin\Theta, \tag{1}$$

where x, y, and Θ are the radial, axial, and angular coordinates of the cylindrical system of coordinates; u, v, and w are the displacements in the corresponding directions of the cylindrical system of coordinates; and an overbar indicates

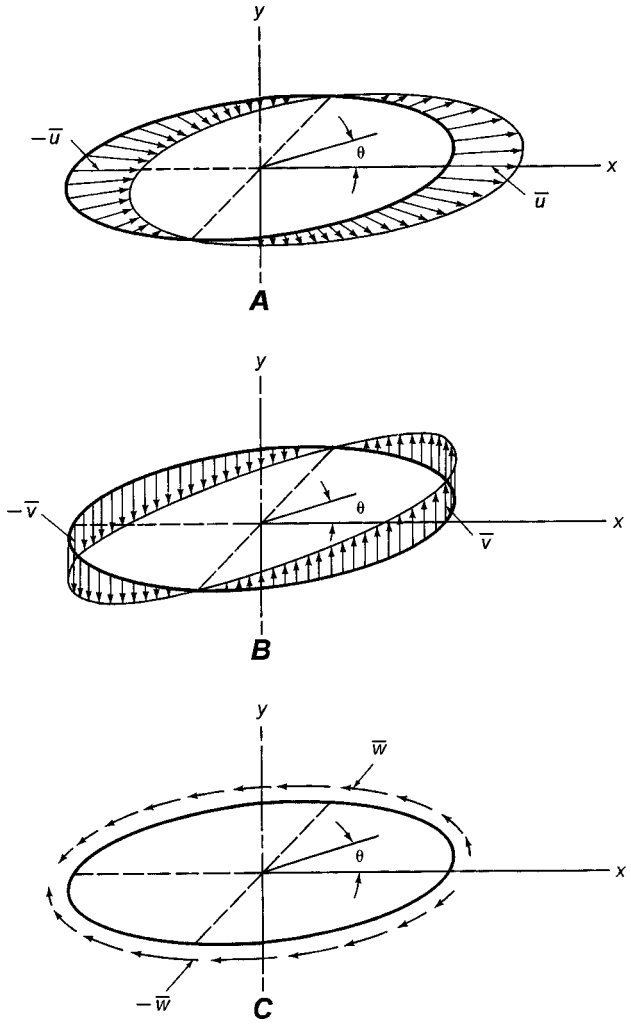

Fig. 4 Schematic representation of the variation of the displacements in the circumferential direction: (a) radial displacement, (b) axial displacement, (c) angular displacement.

the amplitude of the first harmonic in the circumferential direction (Fig. 4).

The following finite element matrices are introduced:

$$\begin{bmatrix} \mathbf{N}_u \\ \mathbf{N}_v \\ \mathbf{N}_w \end{bmatrix} = \begin{bmatrix} N_1 & 0 & 0 & \cdots \\ 0 & N_1 & 0 & \cdots \\ 0 & 0 & N_1 & \cdots \end{bmatrix},$$

$$\begin{bmatrix} \mathbf{N}_{ux} \\ \mathbf{N}_{vx} \\ \mathbf{N}_{wx} \end{bmatrix} = \begin{bmatrix} \frac{\partial N_1}{\partial x} & 0 & 0 & \cdots \\ 0 & \frac{\partial N_1}{\partial x} & 0 & \cdots \\ 0 & 0 & \frac{\partial N_1}{\partial x} & \cdots \end{bmatrix},$$

$$\begin{bmatrix} \mathbf{N}_{uy} \\ \mathbf{N}_{vy} \\ \mathbf{N}_{wy} \end{bmatrix} = \begin{bmatrix} \frac{\partial N_1}{\partial y} & 0 & 0 & \cdots \\ 0 & \frac{\partial N_1}{\partial y} & 0 & \cdots \\ 0 & 0 & \frac{\partial N_1}{\partial y} & \cdots \end{bmatrix}, \tag{2}$$

where N_i are the shape functions of the analyzed finite element; $\mathbf{N}_u$, $\mathbf{N}_v$ and $\mathbf{N}_w$ are row vectors; and indices x and y denote appropriate partial derivatives.

The mass matrix of the fluid takes the following form:

$$\mathbf{M} = \int (\mathbf{N}_c^T \rho \mathbf{N}_c + \mathbf{N}_s^T \rho \mathbf{N}_s) x \, \mathrm{d}x \, \mathrm{d}y, \tag{3}$$

where ρ is the density of the fluid, $\mathbf{N}_c$ and $\mathbf{N}_s$ are the matrices of the shape functions, defined by the following relationship:

$$\begin{bmatrix} u(x,y,\Theta) \\ v(x,y,\Theta) \\ w(x,y,\Theta) \end{bmatrix} = \mathbf{N}_c(x,y)\boldsymbol{\delta}\cos\Theta + \mathbf{N}_s(x,y)\boldsymbol{\delta}\sin\Theta, \tag{4}$$

where $\boldsymbol{\delta}$ is the nodal displacement vector. Explicitly,

$$\mathbf{N}_c = \begin{bmatrix} \mathbf{N}_u \\ \mathbf{N}_v \\ \mathbf{0} \end{bmatrix}, \quad \mathbf{N}_s = \begin{bmatrix} \mathbf{0} \\ \mathbf{0} \\ \mathbf{N}_w \end{bmatrix}. \tag{5}$$

The stiffness matrix of the fluid is

$$\mathbf{K} = \int (\bar{\mathbf{B}}_c^T \rho c^2 \bar{\mathbf{B}}_c + \tilde{\mathbf{B}}_s^T \lambda \tilde{\mathbf{B}}_s + \tilde{\mathbf{B}}_c^T \lambda \tilde{\mathbf{B}}_c) x \, \mathrm{d}x \, \mathrm{d}y, \tag{6}$$

where c is the speed of sound in the fluid, and λ is the penalty parameter for the condition of irrotationality. The matrix $\bar{\mathbf{B}}_c$ relates the volumetric strain with the displacements and is determined from

$$\frac{\partial u}{\partial x} + \frac{\partial v}{\partial y} + \frac{u}{x} + \frac{1}{x}\frac{\partial w}{\partial \Theta} = \bar{\mathbf{B}}_c(x,y)\boldsymbol{\delta}\cos\Theta. \tag{7}$$

Explicitly,

$$\bar{\mathbf{B}}_c = \mathbf{N}_{ux} + \mathbf{N}_{vy} + \frac{1}{x}\mathbf{N}_u + \frac{1}{x}\mathbf{N}_w. \tag{8}$$

The matrices $\tilde{\mathbf{B}}_s$ and $\tilde{\mathbf{B}}_c$ are used to characterize the rotation and are defined from

$$\begin{bmatrix} \frac{\partial w}{\partial y} - \frac{1}{x}\frac{\partial v}{\partial \Theta} \\ \frac{1}{x}\frac{\partial u}{\partial \Theta} - \frac{\partial w}{\partial x} - \frac{w}{x} \\ \frac{\partial v}{\partial x} - \frac{\partial u}{\partial y} \end{bmatrix} = \tilde{\mathbf{B}}_s(x,y)\boldsymbol{\delta}\sin\Theta + \tilde{\mathbf{B}}_c(x,y)\boldsymbol{\delta}\cos\Theta. \tag{9}$$

Thus

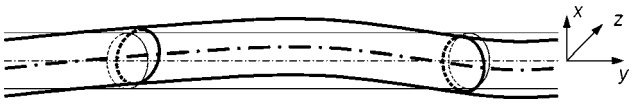

Fig. 5 Schematic diagram of the vibrating pipe.

$$\widetilde{\mathbf{B}}_s = \begin{bmatrix} \mathbf{N}_{wy} + \frac{1}{x}\mathbf{N}_v \\ -\frac{1}{x}\mathbf{N}_u - \mathbf{N}_{wx} - \frac{1}{x}\mathbf{N}_w \\ \mathbf{0} \end{bmatrix}, \quad \widetilde{\mathbf{B}}_c = \begin{bmatrix} \mathbf{0} \\ \mathbf{0} \\ \mathbf{N}_{vx} - \mathbf{N}_{uy} \end{bmatrix}. \tag{10}$$

Now the eigenproblem for this model is solved and the obtained eigenmodes are used for the construction of numerically simulated interference patterns.

3 Holographic Interferometry of Fluids

Schematic diagrams of the analyzed vibrating pipe and optical experimental setup are presented in Fig. 5 and Fig. 6. The laser beam is split by a beamsplitter, forming the object and reference beams. The object beam is collimated by a spherical lens 1 and a parabolic mirror 1 before passing through the investigated fluid in a vibrating pipe. Then the diameter of the beam is reduced by the combination of the parabolic mirror 2 and the spherical lens 2. They image the investigated fluid onto the holographic film. The reference beam passes through mirrors 2 and 3 and then is expanded by a lens 3. It illuminates the holographic film interfering with the object beam.

The phase of the light from the laser beam, $\Psi\ (x,y,t)$, can be expressed as[12,23]

$$\Psi(x,y,t) = \frac{2\pi}{\lambda}\int [n_0 - n_{\text{flow}}(x,y,z,t)]\,\mathrm{d}z, \tag{11}$$

where x, y, z are the orthogonal Cartesian coordinates indicated in Fig. 5, λ is the wavelength of the laser beam, and n_0 and $n_{\text{flow}}(x,y,z,t)$ are the refractive indexes in the initial and flow conditions, respectively. The refractive index is expressed by the Gladstone-Dale relation[11,12]:

$$n(x,y,z,t) = 1 + \beta\frac{\rho(x,y,z,t)}{\rho_0}, \tag{12}$$

where ρ_0 is the density of the fluid (constant in equilibrium), β is the constant of proportionality, $\rho(x,y,z,t)$ is the density of the fluid, and β/ρ_0 is the specific refractivity, or Gladstone-Dale constant.[12] In our case it follows from Eq. (12) that

$$n_0 = 1 + \beta \tag{13}$$

and

$$n_{\text{flow}}(x,y,z,t) = 1 + \beta\frac{\rho_{\text{flow}}(x,y,z,t)}{\rho_0}. \tag{14}$$

From the previous relationships and Eq. (11) it follows that

$$\Psi(x,y,t) = \Psi_0\int \mathrm{d}z - k\int \rho_{\text{flow}}(x,y,z,t)\,\mathrm{d}z, \tag{15}$$

where the constants Ψ_0 and k are expressed as

$$\Psi_0 = \frac{2\pi}{\lambda}\beta, \tag{16}$$

$$k = \frac{2\pi}{\lambda}\frac{\beta}{\rho_0}. \tag{17}$$

The deviation of the density of the fluid from its value in equilibrium is denoted as

$$\widetilde{\rho}(x,y,z,t) = \rho_{\text{flow}}(x,y,z,t) - \rho_0. \tag{18}$$

It is assumed that this deviation is small. Thus

$$|\widetilde{\rho}(x,y,z,t)| \ll \rho_0. \tag{19}$$

Then the phase on the basis of Eqs. (15) and (18) can be expressed as

$$\Psi(x,y,t) = \overline{\Psi_0}(x,y) - k\int \widetilde{\rho}(x,y,z,t)\,\mathrm{d}z, \tag{20}$$

where

$$\overline{\Psi_0}(x,y) = (\Psi_0 - k\rho_0)\int \mathrm{d}z. \tag{21}$$

When Eq. (19) is in force, the condition of continuity of the fluid takes the form

$$\frac{\partial\rho_{\text{flow}}(x,y,z,t)}{\partial t} = -\rho_0\frac{\partial\varepsilon_v(x,y,z,t)}{\partial t}, \tag{22}$$

where $\varepsilon_v(x,y,z,t)$ is the volumetric strain. Further, it is assumed that the density and the displacements of the fluid are harmonically varying in time. Thus the fields of the density and the volumetric strain can be simplified to the form

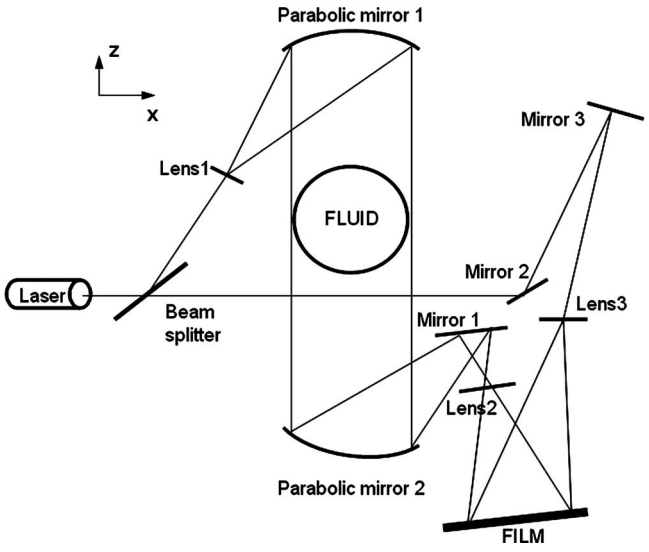

Fig. 6 Schematic diagram of the optical setup.

$$\rho_{\text{flow}}(x,y,z,t) = \rho_0 + \tilde{\rho}^*(x,y,z)\,\sin\omega t \tag{23}$$

and

$$\varepsilon_v(x,y,z,t) = \tilde{\varepsilon}_v^*(x,y,z)\,\sin\omega t, \tag{24}$$

where the angular frequency ω coincides with the eigenfrequency of oscillations of the appropriate eigenmode, $\tilde{\rho}^*(x,y,z)$ is the eigenmode of the density variation, and $\tilde{\varepsilon}_v^*(x,y,z)$ is the eigenmode of volumetric strain. Equation (22) together with Eqs. (23) and (24) yields

$$\tilde{\rho}^*(x,y,z) = -\rho_0\tilde{\varepsilon}_v^*(x,y,z). \tag{25}$$

Then the phase on the basis of Eq. (20) can be expressed as

$$\Psi(x,y,t) = \overline{\Psi_0}(x,y) + k\rho_0\int \tilde{\varepsilon}_v^*(x,y,z)\,\mathrm{d}z\,\sin\omega t. \tag{26}$$

Thus the intensity of the laser beam in the hologram plane is a function of $\tilde{\varepsilon}_v^*(x,y,z)$. Now, the volumetric strains must be determined from the field of displacements. That is because conventional finite-element techniques are based on the approximation of nodal displacements, not strains.

4 Determination of the Volumetric Strains

The amplitudes of circumferential variation of nodal volumetric strains for the appropriate eigenmodes are determined using the procedure of conjugate approximation.[24] The numerical model of the system is based on the approximation of nodal displacements via the shape functions. First, the amplitudes of the circumferential variation of the volumetric strains $\varepsilon_{v\,\cos}$ at the points of numerical integration of the finite element are calculated in the usual way:

$$\varepsilon_{v\,\cos} = \bar{\mathbf{B}}_c(x,y)\boldsymbol{\delta}_0, \tag{27}$$

where $\boldsymbol{\delta}_0$ is the vector of nodal displacements of the eigenmode. Then the field of the amplitudes of the circumferential variation of the volumetric strain is calculated using the procedure of conjugate approximation, which produces the following system of linear algebraic equations:

$$\int\int \hat{\mathbf{N}}^T\hat{\mathbf{N}}\,2\pi x\,\mathrm{d}x\,\mathrm{d}y\cdot\delta_v = \int\int \hat{\mathbf{N}}^T\varepsilon_{v\,\cos}\,2\pi x\,\mathrm{d}x\,\mathrm{d}y, \tag{28}$$

where $\boldsymbol{\delta}_v$ is the vector of nodal values of ε_{vcos} (the eigenmode of the amplitudes of the circumferential variation of the volumetric strains), $\hat{\mathbf{N}}=[N_1 \quad N_2 \quad \cdots]$ is the row of the shape functions of the finite element. Now, the obtained field of volumetric strain can be used in the numerical procedure for the construction of the interference pattern of fringes.

5 Generalized Abel Transform

As mentioned previously, reconstruction of digital holograms for objects characterized by axisymmetric geometry requires incorporation of the Abel transform into the optical relationships governing the formation of fringes. The penetration of the laser beam into the liquid in our problem (in the z-direction) is related to the radial coordinate r [Fig. 7(a)]. The relationship between the variations dz and dr is

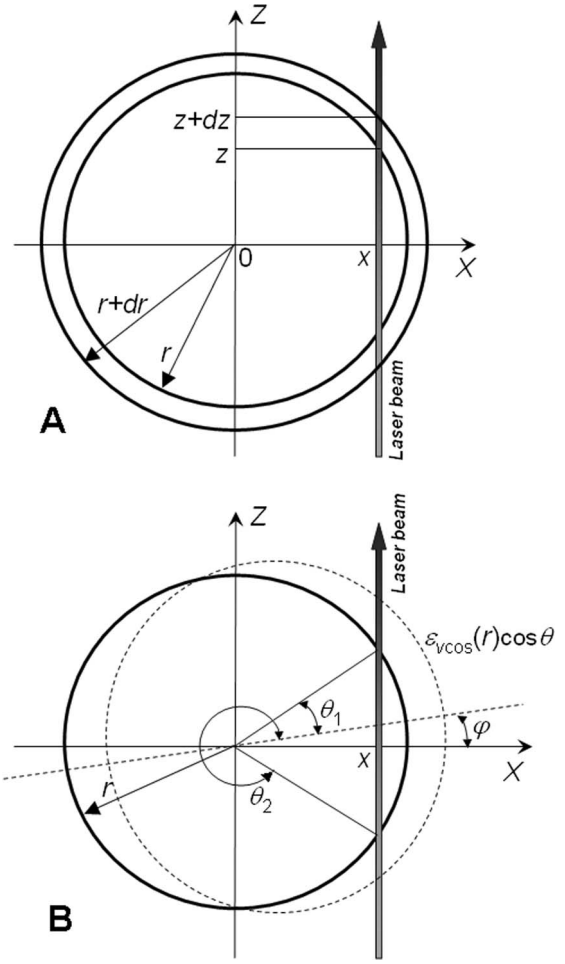

Fig. 7 Generalized Abel transform: (a) change of variables, (b) variation of volumetric strain.

the subject of the classical Abel transform.[3,9,11] The incorporation of the viewing direction is performed by assuming that the pipe is turned by an angle φ and thus the previously used angular coordinate Θ is replaced by $\Theta+\varphi$, as is illustrated in detail in Fig. 7(b). The dashed line in Fig. 7 represents the eigenmode of the volumetric strain; $\varepsilon_{v\,\cos}(r)\,\cos\theta$ stands for the first eigenmode of the volumetric strain. If the angle φ were equal to zero, the shape of the first eigenmode would coincide with the one presented in Fig. 4. When φ is not equal to zero, the angles of intersection between the laser beam and the radius r (under the assumption that the oscillations around the state of equilibrium are small) are denoted as θ_1 and θ_2. These angles can be determined from the following relationship:

$$\tan(\Theta+\varphi) = \frac{z}{x} = \frac{\pm(r^2-x^2)^{1/2}}{x}. \tag{29}$$

Now, the two solutions are denoted as

$$(\Theta+\varphi)_1 = \tan^{-1}\frac{(r^2-x^2)^{1/2}}{x},$$

$$(\Theta+\varphi)_2=\tan^{-1}\frac{-(r^2-x^2)^{1/2}}{x}. \tag{30}$$

Then the generalized Abel transform for the analyzed problem of circumferential vibration takes the following form:

$$\Phi(x,y,\varphi)=\int_x^\infty \varepsilon_{v\,\cos}(r,y)\{\cos[(\Theta+\varphi)_1-\varphi]+\cos[(\Theta+\varphi)_2-\varphi]\}\frac{r\,dr}{(r^2-x^2)^{1/2}}. \tag{31}$$

It can be noted that no interference fringes are formed at $\varphi=\pi/2$, due to the oddness of the trigonometric functions:

$$\Phi\left(x,y,\frac{\pi}{2}\right)=\int_x^\infty \varepsilon_{v\,\cos}(r,y)\left(\sin\left\{\tan^{-1}\left[\frac{-(r^2-x^2)^{1/2}}{x}\right]\right\}+\sin\left\{\tan^{-1}\left[\frac{(r^2-x^2)^{1/2}}{x}\right]\right\}\right)\frac{r\,dr}{(r^2-x^2)^{1/2}}=0. \tag{32}$$

The fact that no interference fringes are observed when the viewing direction is $\pi/2$ imposes definite requirements on the experimental setup. Measurements in all viewing directions must be performed in order to determine the maximum fringe density. The symmetry of the problem reduces the interval of possible viewing directions to $\varphi\in[0;\pi[$. In practice a number of measurements must be performed at incremental discrete values of φ. The smaller is the selected step of φ, the better is the reconstruction of the fringe pattern containing the largest number of fringes.

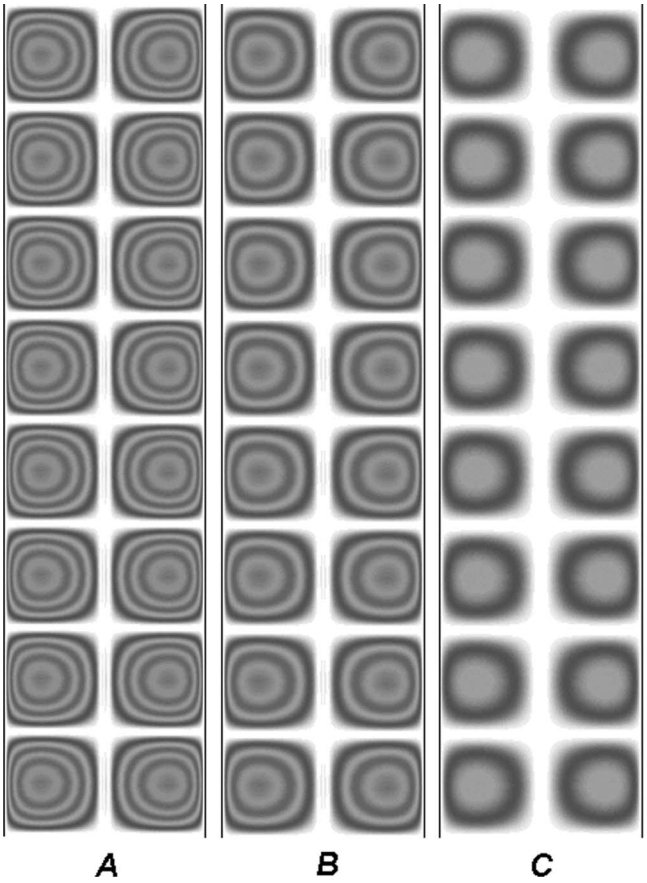

Fig. 8 Numerically simulated pattern of fringes for the fluid in the first circumferential vibration mode: (a) viewing direction $\varphi=0$; (b) viewing direction $\varphi=\pi/4$; (c) viewing direction $\varphi=7\pi/18$.

6 Numerical and Experimental Results

The problem with axisymmetric geometry in a rectangular domain is now analyzed. The right boundary is rigid (corresponding to the wall of the tube), and the displacements normal to it are set equal to zero (marked as black lines in Figs. 8 and 9). The left boundary is the axis of symmetry, and all the displacements on it are set to zero. Both left and right images of the tube are shown in Figs. 8 and 9 for clarity; the axis of symmetry is located at the center of every drawing. Periodic boundary conditions on the upper and lower surfaces are assumed: the displacements on those surfaces for the same values of the radial coordinate are assumed equal. Numerically simulated time-average interference patterns of fluid vibration for the viewing direction $\varphi=0$ are presented in Figs. 8(a) and 9(a). Clearly, the number of developed interference fringes depends from the viewing direction [Figs. 8(b), 9(b), 8(c), and 9(c)]. When the viewing direction is $\pi/2$, no interference fringes are observed and the viewing area in the hologram is white. Procedures for numerical construction of patterns of fringes are discussed in detail in Ref. 25.

The number of fringes and their shapes carry important information about the volumetric strain of the fluid. In general, the larger is the number of fringes, the higher is the volumetric strain. The properties of the analyzed system depend on many parameters. It would be a rather complex task to relate the number of experimentally produced fringes to the numerical values of volumetric strain. Alternatively, patterns of fringes can be mimicked using computational tools (as is done in Figs. 8 and 9). The distribution and magnitude of the volumetric strain (calculated using finite-element techniques) is one of the main parameters affecting the number of fringes and their shape. Variation of system's parameters can help to correlate numerically mimicked and experimentally produced patterns of fringes; that is a typical application of hybrid numerical-experimental techniques.[7,8] Then the field of volumetric strain in the experimentally analyzed system can be estimated from the numerical model of the system.

Silver halide photomaterial PFG-01 (www.geola.lt) is used for recording experimental holograms. The grain size of the photomaterial is 40 nm; the resolution, >3000 lines/mm; the spectral sensitivity range, 600 to 680 nm. The light source used is a He-Ne continuous laser LG-38 with wavelength 0.63 μm; and power 50 mW. The distance between the source and the object is 300 mm; the distance between the object and the hologram plane is 100 mm; the exposure time is 10 s. The analyzed fluid is a saline physiological solution. It is filled into a laboratory glass tube of internal diameter 10 mm. A steel wire waveguide of diameter 0.5 mm is placed along the axis of the tube (filled with the fluid). One end of the waveguide is fixed to the bottom of the tube, and the other end to the previously described ultrasonic probe system. The fre-

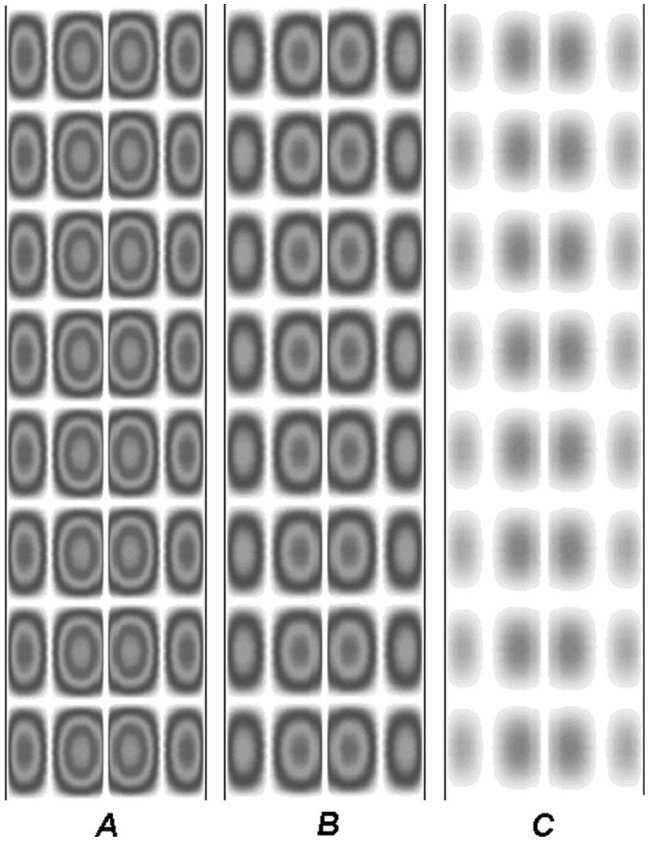

Fig. 9 Numerically simulated pattern of fringes for the fluid in the second circumferential vibration mode: (a) viewing direction $\varphi=0$; (b) viewing direction $\varphi=\pi/4$; (c) viewing direction $\varphi=7\pi/18$.

quency of excitation is 55 kHz. The experimentally produced laser holographic interferogram is presented in Fig. 10.

An important conclusion can be reached with regard to the previously described ultrasonic probe system. Though laser fluid holography is a powerful optical technique ideally suited for experimental investigation of such systems, one must have in mind that laser holograms must be constructed for different viewing directions. Otherwise the number of developed fringes may not represent the maximum volumetric strains, which in its turn may have lethal effects in treatment procedures.

7 Concluding Remarks

A numerical model for the calculation of fluid vibrations in the circumferential direction in axisymmetric geometry has been developed. The procedure for the calculation of nodal values of the amplitudes of the circumferential variation of the volumetric strain is presented. The obtained volumetric strains are used for the numerical construction of the interference patterns, exploiting the generalized Abel transform. The fact that the number of developed fringes in a fluid vibrating in the circumferential direction depends on the direction of observation imposes certain requirements on the setup of the experimental analysis. A number of measurements must be performed in different viewing directions before any conclusions can be reached about the volumetric strains in the analyzed fluid. That is important for the biomedical application of ultrasonic probes described in this paper.

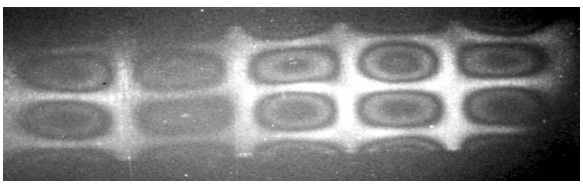

Fig. 10 Experimentally produced time-average laser holographic interferogram of vibrating fluid.

References

1. J. Binney and S. Tremaine, *Galactic Dynamics*, Princeton Univ. Press, Princeton (1987).
2. K. G. Hollingsworth and M. L. Johns, "Spatially resolved emulsion droplet sizing using inverse Abel transforms," *J. Magn. Reson.* **176**(1), 71–78 (2005).
3. F. Yousefian and M. Lallemand, "Inverse radiative analysis of high-resolution infrared emission data for temperature and species profiles recoveries in axisymmetric semi-transparent media," *J. Quant. Spectrosc. Radiat. Transf.* **60**(6), 921–931 (1998).
4. B. A. Vanderwege, C. J. O'Brien, and S. Hochgreb, "Quantitative shearography in axisymmetric gas temperature measurements," *Opt. Lasers Eng.* **31**(1), 21–39 (1999).
5. H. Asano, N. Takenaka, T. Fujii, E. Nakamatsu, Y. Tagami and K. Takeshima, "Image processing methods to obtain symmetrical distribution from projection image," *Appl. Radiat. Isot.* **61**(4), 625–630 (2004).
6. E. Simonneau, A. M. Varela, and C. Munoz-Tunon, "Spectral inversion of the generalized Abel integral transform," *J. Quant. Spectrosc. Radiat. Transf.* **49**(2), 149–156 (1993).
7. D. Rittel, "A hybrid experimental–numerical investigation of dynamic shear fracture," *Eng. Fract. Mech.* **72**(1), 73–89 (2005).
8. A. Holstein, L. Salbut, M. Kujawinska, and W. Juptner, "Hybrid experimental–numerical concept of residual stress analysis in laser weldments," *Exp. Mech.* **41**(4), 343–350 (2001).
9. C. M. Vest, *Holographic Interferometry*, Chap. 3, Wiley, New York (1979).
10. W. Lauterborn and A. Vogel, "Modern optical techniques in fluid mechanics," *Annu. Rev. Fluid Mech.* **16**, 223–244 (1984).
11. A. Houwing, K. Takayama, K. Koremoto, T. Hashimoto, and H. Mitobe, "Finite fringe analysis of two dimensional and axially-symmetric flows," *Proc. SPIE* **398**, 174–180 (1983).
12. J. H. Han, A. Kennaugh, and D. I. A. Poll, "Visualization of non-equilibrium dissociating flows," *J. Aerosp. Eng.* **211**(G5), 295–305 (1997).
13. L. Bruno, L. Pagnotta, and A. Poggialini, "A full-field method for measuring residual stresses in optical fiber," *Opt. Lasers Eng.* **44**(6), 577–588 (2006).
14. G. P. Zou, N. Cheraghi, and F. Taheri, "Fluid-induced vibration of composite natural gas pipelines," *Int. J. Solids Struct.* **42**(3–4), 1253–1268 (2005).
15. H. R. Oz and H. Boyaci, "Transverse vibrations of tensioned pipes conveying fluid with time-dependent velocity," *J. Sound Vib.* **236**(2), 259–276 (2000).
16. M. Ragulskis, A. Fedaravicius, and K. Ragulskis, "Harmonic balance method for FEM analysis of fluid flow in a vibrating pipe," *Commun. Numer. Methods Eng.* **22**(4), 347–356 (2006).
17. R. Rabiner and B. A. Hare, "Ultrasonic device for tissue ablation and sheath for use therewith," U.S. Patent No. 6,524,251 (2003).
18. H. M. Alliger and D. J. Ciervo, "Ultrasonic device for applying cavitation forces," U.S Patent No. 49,20,954 (1990).
19. A. Palevicius, K. Ragulskis, A. Bubulis, V. Ostasevicius, and M. Ragulskis, "Development and operational optimization of micro spray system," *Proc. SPIE* **5390**, 429–438 (2004).
20. V. Souday, P. Asfar, and C. M. Muth, "Diagnosis and treatment of gas embolism," *Reanimation* **12**(7), 482–490 (2003).
21. N. F. Iershov and G. G. Shahvierdi, *The Method of Finite Elements in the Problems of Hydrodynamics and Hydroelasticity*, Sudostroenie, Leningrad (1984).
22. O. C. Zienkiewicz and R. L. Taylor, *The Finite Element Method, Volume 3. Fluid Dynamics*, Wiley, New York (2000).
23. M. Ragulskis, A. Palevičius, A. Fedaravičius, and L. Ragulskis, "Applicability of time-average fluid holography for analysis of propagating waves," *Opt. Eng.* **44**(10), 105801 (2005).

24. M. Ragulskis and L. Ragulskis, "Conjugate approximation with smoothing for hybrid photoelastic and FEM analysis," *Commun. Numer. Methods Eng.* **20**(8), 647–653 (2004).
25. M. Ragulskis, A. Palevičius, and L. Ragulskis, "Plotting holographic interferograms for visualization of dynamic results from finite-element calculations," *Int. J. Numer. Methods Eng.* **56**(11), 1647–1659 (2003).

Minvydas Ragulskis received his PhD degree in 1992 from Kaunas University of Technology, Lithuania. He is currently a professor in the Department of Mathematical Research in Systems, Kaunas University of Technology. His research interests are numerical analysis and dynamical systems. He is a member of SIAM and SEM.

Arvydas Palevicius received his PhD degree in 1985 from Kaunas University of Technology, Lithuania. He is currently a professor in the Department of International Studies, Kaunas University of Technology. His research interests are laser holographic interferometry and microlithography. He is a member of SPIE and SEM.

Liutauras Ragulskis received his PhD degree in 1987 from Kaunas University of Technology, Lithuania. He has been with Lithuanian Institute of Energy since 1988 and with Vytautas Magnus University since 1991, where he is currently a research associate in the Department of Informatics. His research interests are programming and application of finite-element methods.

Algimantas Bubulis received his PhD degree in 1979 from Kaunas University of Technology, Lithuania. He is currently a professor at the Institute of Piezomechanics, Kaunas University of Technology. His research interests are piezomechanics and fluid dynamics.